ORIGINAL PAPER DOI: 10.5603/oj.98652

Quantitative evaluation of anterior chamber parameters using anterior segment optical coherence tomography in primary angle closure mechanisms in Caucasian eyes

Andrzej Sawicki, Agnieszka Wilkos-Kuc, Tomasz Zarnowski

Department of Diagnostics and Microsurgery of Glaucoma, Medical University of Lublin, Poland

ABSTRACT

BACKGROUND: The purpose of this study was to evaluate different mechanisms of primary angle closure disease (PACD) and quantify anterior chamber parameters in these mechanisms using anterior segment optical coherence tomography (ASOCT) in a Caucasian population.

DESIGN: Hospital-based cross-sectional observational study/Clinic based study.

PARTICIPANTS: 144 eyes (73 patients) with newly diagnosed primary angle closure disease (PACD), classified into three subtypes: primary angle closure suspect (PACS), primary angle closure (PAC), and primary angle closure glaucoma (PACG), were enrolled to the study.

MATERIAL AND METHODS: Participants underwent ASOCT (SS-1000 CASIA, Tomey Corporation, Nagoya, Japan) under the same standardized dark room conditions. ASOCT images were categorized into one of 4 groups based on the angle-closure mechanisms: pupillary block (PB), plateau iris configuration (PIC), thick peripheral iris (TPI), and large lens vault (LLV). Anterior chamber depth (ACD), anterior chamber area (ACA), anterior chamber volume (ACV), anterior chamber width (ACW), iris area (IA), iris curvature (IC), iris curvature area (ICA), iris thickness (IT750, IT2000), lens vault (LV), pupil diameter (PD), angle opening distance (AOD500, AOD750), angle recess area (ARA 500, ARA750), trabecular iris angle (TIA500, TIA750) and trabecular iris space area (TISA500, TISA750) were determined using 360o SS-OCT viewer software (version 5.0, Tomey, Nagoya, Japan).

RESULTS: Among 144 examined eyes, 83 eyes (57.6%) were classified as PB, 42 eyes (29.2%) as PIC, 14 eyes (9.7%) as TPI, and 5 eyes (3.5%) as LLV. 73.6 % had a single underlying PAC mechanism, and the rest had more than one (combined mechanism) of PAC. Anterior chamber parameters (ACD, ACA, ACV) were the highest in the PIC group and the lowest in the LLV group. Angle parameters (AOD 500, AOD 750, TIA 750; SSAngle 500; SSAngle 750) showed the strongest relevance and were the highest in the PIC group and the lowest in the TPI group. LV was the greatest in the LLV and the lowest in the TPI and PIC groups. Axial length (AL) was the largest in PIC, followed by PB, and the smallest in the LLV group.

CONCLUSION: Anterior chamber and anterior chamber angle parameters showed significant differences between the four angle closure mechanisms. Identifying the angle closure mechanisms could lead to better disease management by individualizing the treatment.

KEY WORDS: anterior chamber parameters; anterior chamber angle parameters; anterior segment optical coherence tomography; ASOCT; primary angle closure suspects; PACS; primary angle closure; PAC; primary angle closure glaucoma; PACG; angle closure mechanisms

Ophthalmol J 2024; Vol. 9, 68–76

CORRESPONDING AUTHOR:
Andrzej Sawicki, Department of Diagnostics and Microsurgery of Glaucoma, Medical University of Lublin, Poland; e-mail: andrzej.jerzy.sawicki@gmail.com

INTRODUCTION

Glaucoma is the leading cause of global irreversible blindness. It is estimated that the number of people with glaucoma worldwide will increase from 64,3 million in 2013 to 111,8 million in 2040 [1]. Although primary open-angle glaucoma (POAG) is more common, primary-angle closure glaucoma (PACG) is more severe and more likely to result in blindness if not treated properly. Pupillary block is the main mechanism in the pathogenesis of primary angle closure. Laser peripheral iridotomy (LPI), which eliminates pupillary block, is the standard treatment for primary angle closure (PAC/PACD). However, LPI may not always be the best treatment for all subtypes of angle closure. Many eyes have residual angle closure after LPI; thus, other mechanisms of angle closure, such as plateau iris configuration, thick peripheral iris, and thick, anteriorly positioned lens, are considered. Identifying these mechanisms could lead to better disease management by individualizing treatment. The aim of this study is to qualitatively recognize and quantitatively evaluate the four main PAC mechanisms using ASOCT imaging.

The prevalence of PACG varies among different races; among Caucasians, it is estimated to be 0.4% [2], and among Asians, it is 1.09% [3]. The highest rate is observed in Inuits, which is 20-40 times higher than that of Caucasians [4]. PACG is the only type of glaucoma that could be entirely prevented if it is properly diagnosed and treated.

MATERIAL AND METHODS

144 eyes of 73 consecutive patients with primary angle-closure disease (PACD) who visited the Department of Diagnostics and Microsurgery of Glaucoma of Lublin and met the inclusion criteria were enrolled in the study.

All eyes were newly diagnosed cases and had no previous ophthalmic history. We excluded patients who either were using glaucoma medications or had a history of intraocular surgery, such as cataract surgery, laser peripheral iridotomy (LPI), or laser iridoplasty.

Diagnosis of primary angle-closure disease (PACD) was based on the gonioscopy.

The study was approved by the Bioethics Committee of the Medical University of Lublin, Poland, and conducted in accordance with the tenets of the Declaration of Helsinki. Written informed consent was obtained from all participants.

All participants underwent a complete ophthalmic examination, including a review of medical history, refraction, measurement of best corrected visual acuity (BCVA), slit lamp biomicroscopy, Goldmann applanation tonometry, gonioscopy, fundus examination using 78-diopter lens, central corneal thickness (CCT), visual field (VF) test (Humphrey Field Analizer, Swedish Interactive Threshold Algorithm 24-2, Carl Zeiss Meditec Inc.), axial length measurement (IOL Master 500, Carl Zeiss Meditec Inc.), OCT imaging of macula and optic disc/retinal nerve fiber layer (Zeiss Cirrus 4000) and ASOCT (SS-1000 CASIA, Tomey Corporation, Nagoya, Japan).

Gonioscopy

Gonioscopy was performed in a dark room by a glaucoma specialist using a Zeiss style four mirror goniolens (Model G-4, Volk Optical, Mentor, OH, USA). The Shaffer grading system was used to evaluate the angle. Both static and indentation gonioscopy were done to determine the presence of iridotrabecular contact (ITC) and/or PAS.

PACD was diagnosed when an eye had an occludable angle (pigmented posterior trabecular was not visible on non-indentation gonioscopy for at least 180° in the primary position). All eyes were then classified into one of 3 groups: primary angle closure suspect (PACS), primary angle closure (PAC), or primary angle closure glaucoma (PACG), as follows (Tab. 1).

Anterior segment optical coherence tomography (ASOCT)

Anterior segment optical coherence tomography (ASOCT) is a rapidly developing technology which allows us to perform precise qualitative and quantitative assessment of the anterior segment. ASOCT

Table 1. Classification of primary angle-closure disease (PACD) in the present study

Subtypes of PACD	Definition
Primary angle closure suspect (PACS)	≥ 180° iridotrabecular contact (ITC), **and** no PAS, **and** IOP ≤ 21 mm Hg, **and** no glaucomatous optic neuropathy
Primary angle-closure (PAC)	≥ 180° iridotrabecular contact, **and** presence of PAS and/or IOP > 21 mm Hg, **and** no glaucomatous optic neuropathy
Primary angle-closure glaucoma (PACG)	≥ 180° iridotrabecular contact, **and** presence of PAS and/or IOP > 21 mm Hg, **and** glaucomatous optic neuropathy

IOP — intraocular pressure

SS-1000 Casia provides 3D scans which consists of 128 meridional radial scans with the scanning depth of 16 mm. It has been proved these measurements are precise, objective with high level of reproducibility [5–7].

All participants were subjected to ASOCT imaging (SS-1000 CASIA, Tomey Corporation, Nagoya, Japan) with the patient staying in a sitting position, before any contact procedure, under standardized dark conditions. To obtain the full scan of the anterior chamber, the upper and lower eyelids were gently moved, avoiding applying pressure on the globe. Each scan consisted of 128 radial B scans (16 mm x 6 mm) and was assessed, paying special attention to the quality of the image. The 360o SS-OCT viewer software (version 5.0, Tomey, Nagoya, Japan) was used to process the scans; the only user was marking the location of the scleral spur. Only eyes with the visible/well-determined scleral spur were enrolled in the study. The circumference of the anterior chamber angle was divided into four sectors: nasal, temporal, superior, and inferior. Four scans (11.25° increments) of each sector were analyzed.

All ASOCT images were then categorized into one of the 4 groups based on the angle closure mechanisms (PB, PIC, TPI, LLV) by independent investigators (A.S., A.W.K.). In the case of the scan revealing more than one PAC mechanism, the dominant mechanism of angle closure was specified. If there was disagreement between investigators, images were reviewed, and consensus was made.

Classification of the angle closure mechanisms

Images were categorized depending on which one of the 4 angle closure mechanisms was involved: pupillary block (PB), plateau iris configuration (PIC), thick peripheral iris (TPI), and large lens vault (LLV).

1. Pupillary block (PB) was characterized by a convex forward iris profile, giving the typical bombe appearance, very small zone of iris lens contact in the center and shallow peripheral anterior chamber. PB is considered as the leading mechanism in the pathogenesis of PAC.
2. Eyes with plateau iris configuration (PIC) showed the peripheral iris arising from its root in apposition or in close proximity to the angle wall and then turning sharply away from the angle towards the visual axis. The central iris plane was flat, the central anterior chamber was relatively deep, but the peripheral anterior chamber was shallow.
3. In this ASOCT-based study, the plateau iris configuration refers strictly to the specific shape of the iris observed on the ASOCT scans.
4. Thick peripheral iris (TPI) was characterized by a thick iris with folds situated peripherally. The central anterior chamber was relatively deep, while the angle was crowded.
5. Eyes with a large lens vault (LLV) showed a lens that pushed the iris forward, resulting in a small anterior chamber volume and markedly reduced space between the iris and the corneal angle. The iris in eyes with LLV appeared to drape the anterior surface of the lens, giving it a volcano-like configuration.

Quantitative measurements of an ASOCT image

ASOCT images can be used to obtain various parameters. They represent various aspects of anteri-

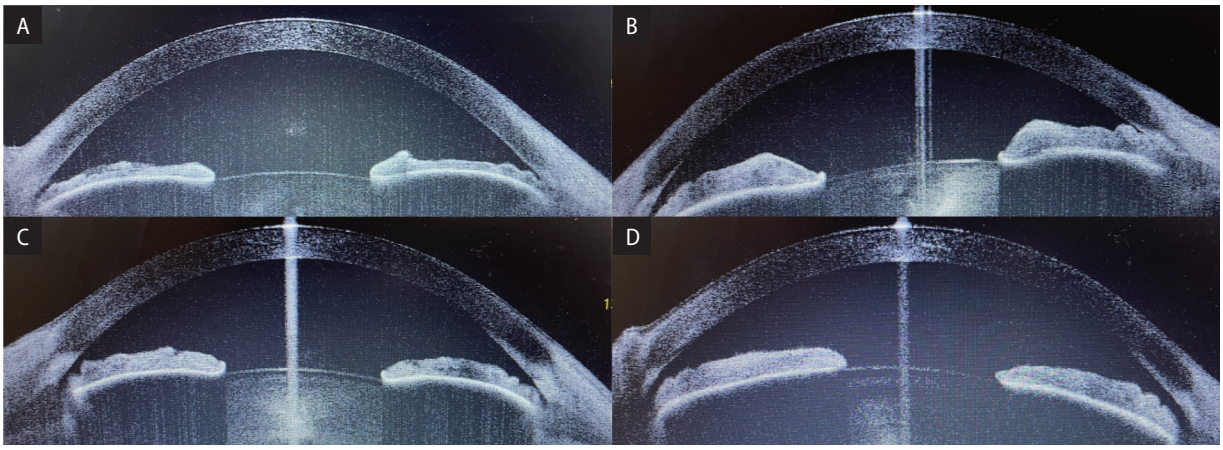

FIGURE 1. Anterior segment optical coherence tomography (ASOCT) scans showing the four mechanisms of primary angle closure. **A.** Plateau iris configuration (PIC); **B.** Thick peripheral iris (TPI); **C.** Pupillary block (PB); **D.** Large lens vault (LLV)

Table 2. Anterior segment optical coherence tomography (ASOCT) parameters	
Anterior chamber depth (ACD)	Distance from the corneal endothelium to the anterior surface of the lens
Anterior chamber area (ACA)	Cross sectional area of the anterior chamber bounded by the posterior surface of the cornea, anterior surface of the iris and anterior surface of the lens
Anterior chamber volume (ACV)	Calculated by software by rotating the ACA 360° around the vertical axis
Anterior chamber width (ACW)	Distance between two scleral spurs
Angle opening distance (AOD500, AOD750)	Perpendicular distance between the trabecular meshwork and the iris at the distance 500 or 750 μm anterior to the sclera spur
Angle recess area (ARA500, ARA750)	triangular area bounded by AOD500 or AOD750, the inner corneoscleral wall and the anterior surface of the iris
Trabecular iris angle (TIA500, TIA750))	The degrees of the angle from the apex in the angle recess and the arms of the angle passing through a point 500 or 750 μm anterior to the scleral spur transecting the inner corneal and the point perpendicular to the iris surface
Trabecular iris space area (TISA500, TISA750)	Trapezoidal area with the following boundaries: anteriorly — AOD500 and AOD750 respectively, posteriorly — a line perpendicular to the corneoscleral wall drawn from the scleral spur to the opposing iris, superiorly — the inner corneoscleral wall, inferiorly — the anterior iris surface
Iris area (IA)	Cross-sectional area of the iris from the scleral spur to the pupil
Iris curvature (IC)	Calculated by the software, defined as the perpendicular distance from the line connecting the most central and the most peripheral points of the iris pigment epithelium to the posterior iris surface at the point of the greatest iris convexity
Iris thickness (IT750, IT2000)	Measured at 750 or 2000 μm anterior to the scleral spur
Lens vault (LV)	Perpendicular distance between the anterior surface of the lens and the horizontal line connecting to scleral spurs
Scleral spur (SS)	The point of which the curvature of the angle-wall inner surface changed noticeably creating an inward protrusion of the sclera

or segment anatomic characteristics, such as the angle, anterior chamber, iris, and lens.

The following parameters were measured:

- AC angle parameters: angle opening distance (AOD500, AOD750), angle recess area (ARA500, ARA750), trabecular iris angle (TIA500, TIA750), trabecular iris space area (TISA500, TISA750);
- AC parameters: anterior chamber depth (ACD), anterior chamber area (ACA), anterior chamber volume (ACV), anterior chamber width (ACW);
- iris parameters: iris area (IA), iris curvature (IC), iris curvature area (ICA), iris thickness (IT750, IT2000);
- lens vault (LV);
- pupil diameter (PD).

RESULTS

It is well-known that a smaller anterior chamber dimension with a small anterior chamber depth strongly correlates with angle closure [8–10]. Other risk factors are older age, female gender, and Asian ancestry. Main ocular risk factors for angle closure include: a narrower angle, thicker lens, shorter axial length, thicker and more anteriorly positioned lens, smaller corneal diameter, and hypermetropic refraction [11]. Recent ASOCT studies have identified novel parameters associated with angle closure, such as smaller anterior chamber area (ACA) and volume (ACV), narrower anterior chamber width (ACW), greater lens vault (LV), increased iris thickness (IT), iris area (IA) and smaller parameters which define the angle [12].

144 eyes from 73 patients were included for qualitative and quantitative analysis. The majority of patients were female (78.5%), and all patients were Caucasian. The mean age was 67.3 ± 9.5 years. There was no significant difference in age and gender between the four groups.

Out of the 144 eyes, 83 eyes (57.6%) had PB, 42 eyes (29.2%) had PIC, 14 eyes (9.7%) had TPI, and 5 eyes (3.5%) had LLV as the dominant angle closure mechanism. 106 eyes had a single underlying PAC mechanism and 38 had more than one (combined mechanism) of PAC.

The axial length was the largest in PIC (22.57 ± 0.92 mm), followed by PB (22.18 ± 0.76 mm) and the smallest in the LLV g group (21.36 ± 0.77 mm).

Table 3. Comparison of clinical characteristics between different mechanisms of angle closure

		Total	PIC (n = 42)	LLV (n = 5)	PB (n = 83)	TPI (n = 14)	Test	p-value
Gender	Male	31 (21.5)	11 (26.2)	1 (20.0)	17 (20.5)	2 (14.3)	Chi-sq = 1.036	0.793
	Female	113 (78.5)	31 (73.8)	4 (80.0)	66 (79.5)	12 (85.7)		
Age (mean ± SD) (years)	35–88	67.27 (9.48)	67.05 (10.60)	66.80 (5.54)	67.82 (9.25)	64.86 (8.78)	Kruskall-Wallis: W = 1.534	0.675
Refractive error (spherical equivalent)	–4.5–8.75	1.77 (2.14)	1.71 (2.35)	3.10 (1.71)	1.46 (1.94)	3.27 (2.09)	Kruskall-Wallis: W = 11.236	0.011
Axial length (mean ± SD) mm	20.05–24.21	22.21 (0.86)	22.57 (0.92)	21.36 (0.77)	22.18 (0.76)	21.57 (0.65)	Kruskall-Wallis: W = 21.046	< 0.001
MD	–31.02–1.24	–4.03 (5.76)	–2.67 (3.14)	–2.89 (1.41)	–4.71 (6.67)	–4.50 (6.57)	Kruskall-Wallis: W = 3.052	0.384
OCT	53–120	84.16 (13.25)	80.85 (13.65)	87.30 (7.55)	84.04 (12.97)	93.71 (11.30)	Kruskall-Wallis: W = 11.641	0.009
CCT	480–646	552.49 (29.47)	563.10 (36.34)	548.50 (17.78)	547.07 (24.61)	554.29 (30.19)	Kruskall-Wallis: W = 5.237	0.155
VA	0–1	0.75 (0.24)	0.79 (0.22)	0.59 (0.15)	0.74 (0.25)	0.71 (0.26)	Kruskall-Wallis: W = 5.930	0.115

PIC — plateau iris configuration; LLV — large lens vault; PB — pupillary block; TPI — tjhick peripheral block; SD — standard deviation; OCT — optical coherence tomography; CCT — central corneal thickness; VA — visual acuity

The spherical equivalent was the largest in the TPI (3.27 ± 2.09 D) and LLV group (3.10 ± 1.71 D) and the lowest in the PB (1.46 ± 1.94 D) and PIC group (1.71 ± 2.35 D).

Anterior chamber parameters were significantly different among four mechanisms ($p < 0.001$).

The anterior chamber depth (ACD), anterior chamber area (ACA), and anterior chamber volume (ACV) were highest in PIC and lowest in the LLV group. The anterior chamber depth (ACD) was highest in PIC (2.28 ± 0.18 mm) and lowest in the LV group (1.66 ± 0.19 mm).

The anterior chamber area (ACA) was significantly different between the four PAC mechanisms ($p < 0.001$). The ACA was highest in PIC (16.00 ± 2.03 mm^2) and lowest in the LLV group (10.77 ± 1.78 mm^2).

The anterior chamber volume (ACV) was significantly different between the four groups ($p < 0.001$). ACV was the highest in PIC.

(105.33 ± 16.85 mm^3) and the lowest in the LLV group (63.39 ± 16.00 mm^3). The lens vault (LV) was significantly different between the four mechanisms ($p < 0.001$). LV was the greatest (1.24 ± 0.11 mm) in LLV and the lowest in TPI (0.68 ± 0.16 mm) and PIC group (0.71 ± 0.22 mm).

Angle parameters

Statistical analysis showed a significant difference ($p < 0.001$) in AOD500 and AOD750 between the four groups. The highest AOD500 (0.17 ± 0.06 mm) and AOD750 (0.23 ± 0.08 mm) were in the PIC group. ARA500 was the highest in LLV (0.08 ± 0.05 mm^2) and PIC (0.07 ± 0.04 mm^2) and the lowest in the TPI group (0.04 ± 0.02 mm^2). ARA750 was the highest in LLV (0.13 ± 0.08 mm^2) and PIC (0.13 ± 0.05 mm^2) and the lowest in the TPI group (0.07 ± 0.03 mm^2).

Significant differences were observed between groups in TIA500 ($p < 0.009$) and TIA750 ($p < 0.003$) parameters. TIA500 was the greatest in PIC (29.94 ± 14.21) and the lowest in the TPI group (19.96 ± 16.53). TIA750 was the greatest in PIC (21.36 ± 6.29 mm) and the lowest in the TPI group (15.15 ± 5.34).

Statistical analysis showed significant differences between the four groups in TISA500 ($p = 0.007$) and TISA750 ($p = 0.003$). TISA500 was the greatest in the PIC (0.12 ± 0.05 mm^2) and LLV (0.12 ± 0.08 mm^2) and the lowest in the TPI group (0.07 ± 0.03 mm^2).

Iris parameter

The pupil diameter (PD), iris thickness (IT750, IT2000), iris curvature (IC), and iris curvature area (ICA) were significantly different between groups.

PD was the largest (4.09 ± 0.94 mm) in TPI and the smallest in LLV (3.12 ± 0.83 mm) and PIC group (3.29 ± 0.58 mm). IT750 and IT 2000

Table 4. Comparison of angle and anterior chamber segment parameters [mean ± standard deviation (SD)] measured by anterior segment optical coherence tomography (ASOCT) in each mechanism of angle closure

	Level	Total	PIC (n = 42)	LLV (n = 5)	PB (n = 83)	TPI (n = 14)	Test	p-value
Gender	Male	31 (21.5%)	11 (26.2%)	1 (20.0%)	17 (20.5%)	2 (14.3%)	$\chi^2 = 1.036$	0.793
	Female	113 (78.5%)	31 (73.8%)	4 (80.0%)	66 (79.5%)	12 (85.7%)		
Diagnosis	PAC	33 (22.9%)	12 (28.6%)	1 (20.0%)	17 (20.5%)	3 (21.4%)	$\chi^2 = 5.759$	0.451
	PACG	30 (20.8%)	11 (26.2%)	0 (0.0%)	18 (21.7%)	1 (7.1%)		
	PACS	81 (56.2%)	19 (45.2%)	4 (80.0%)	48 (57.8%)	10 (71.4%)		
ACD Endo. [mm]	1.46–2.68	2.09 (0.26)	2.28 (0.18)	1.66 (0.19)	2.04 (0.24)	1.97 (0.25)	Kruskall-Wallis: W = 42.471	< 0.001
CAD [mm]	2.25–3.5	2.89 (0.25)	2.99 (0.22)	2.90 (0.19)	2.88 (0.24)	2.65 (0.21)	Kruskall-Wallis: W= 17.939	< 0.001
PD [mm]	1.95–5.45	3.60 (0.72)	3.29 (0.58)	3.12 (0.83)	3.70 (0.68)	4.09 (0.94)	Kruskall-Wallis: W= 14.951	0.002
LV [mm]	0.28–1.32	0.80 (0.21)	0.71 (0.22)	1.24 (0.11)	0.84 (0.17)	0.68 (0.16)	Kruskall-Wallis: W= 26.160	< 0.001
ACA [mm^2]	8.38–20.61	14.30 (2.57)	16.00 (2.03)	10.77 (1.78)	13.86 (2.42)	13.08 (2.16)	Kruskall-Wallis: W= 35.610	< 0.001
Cornea [mm^3]	–1–188.1	125.87 (21.37)	134.99 (14.48)	131.76 (8.11)	123.42 (20.39)	110.93 (34.04)	Kruskall-Wallis: W= 18.060	< 0.001
A.C. [mm^3]	–1–145.92	89.34 (23.32)	105.33 (16.85)	68.39 (16.00)	85.19 (21.27)	73.47 (27.88)	Kruskall-Wallis: W= 39.920	< 0.001
Iris [mm^3]	–1–44.91	32.04 (6.37)	33.84 (4.86)	33.32 (6.25)	31.40 (6.09)	30.03 (10.42)	Kruskall-Wallis: W= 5.431	0.143
AOD500 [Avg. mm]	0.03–0.33	0.15 (0.06)	0.17 (0.06)	0.16 (0.10)	0.14 (0.05)	0.11 (0.04)	Kruskall- Wallis: W= 17.079	< 0.001
AOD750 [Avg. mm]	0.04–0.53	0.20 (0.08)	0.23 (0.08)	0.19 (0.13)	0.19 (0.07)	0.15 (0.05)	Kruskall-Wallis: W= 19.234	< 0.001
ARA500 [Avg. mm^2]	0.01–0.15	0.06 (0.03)	0.07 (0.04)	0.08 (0.05)	0.06 (0.03)	0.04 (0.02)	Kruskall-Wallis: W= 9.857	0.020
ARA750 [Avg. mm^2]	0.02–0.25	0.11 (0.05)	0.13 (0.05)	0.13 (0.08)	0.10 (0.05)	0.07 (0.03)	Kruskall-Wallis: W= 12.544	0.006
TISA500 [Avg. mm^2]	0.01–0.14	0.06 (0.03)	0.07 (0.04)	0.08 (0.05)	0.06 (0.03)	0.04 (0.02)	Kruskall-Wallis: W = 12.225	0.007
TISA750 [Avg. mm^2]	0.02–0.24	0.10 (0.05)	0.12 (0.05)	0.12 (0.08)	0.10 (0.05)	0.07 (0.03)	Kruskall-Wallis: W = 13.865	0.003
TIA500 [Avg. deg.]	2.13–77.97	25.75 (13.32)	29.94 (14.21)	26.98 (17.69)	24.53 (11.56)	19.96 (16.53)	Kruskall-Wallis: W = 11.666	0.009
TIA750 [Avg. deg.]	5.15–56.39	18.50 (6.89)	21.36 (6.29)	17.66 (11.99)	17.67 (6.69)	15.15 (5.34)	Kruskall-Wallis: W = 16.476	< 0.001
SSAngle-500 [Avg. deg.]	2.83–33.41	16.30 (5.76)	18.66 (5.53)	16.86 (10.26)	15.83 (5.21)	11.76 (4.75)	Kruskall-Wallis: W = 17.196	< 0.001
SSAngle-750 [Avg. deg.]	2.83–35.12	14.53 (5.24)	16.91 (5.30)	13.55 (9.26)	13.95 (4.72)	11.22 (3.78)	Kruskall-Wallis: W = 19.229	< 0.001
IT750 [Avg. mm]	0.23–0.51	0.35 (0.05)	0.35 (0.05)	0.31 (0.06)	0.34 (0.04)	0.40 (0.04)	Kruskall-Wallis: W = 17.786	< 0.001
IT2000 [Avg. mm]	0.19–0.58	0.37 (0.06)	0.35 (0.06)	0.36 (0.07)	0.36 (0.05)	0.46 (0.07)	Kruskall-Wallis: W = 22.796	< 0.001
IC [Avg. mm]	0.13 - 0.47	0.32 (0.06)	0.32 (0.05)	0.37 (0.12)	0.33 (0.06)	0.26 (0.05)	Kruskall-Wallis: W = 13.927	0.003
ICA(+) [Avg. mm^2]	0.3 - 2.05	0.83 (0.25)	0.89 (0.25)	1.02 (0.36)	0.83 (0.22)	0.61 (0.21)	Kruskall-Wallis: W = 16.592	< 0.001
IA [Avg. mm^2]	0.91 - 2.04	1.45 (0.24)	1.49 (0.24)	1.58 (0.13)	1.42 (0.22)	1.44 (0.32)	Kruskall-Wallis: W = 4.427	0.219

PIC — plateau iris configuration; LLV — large lens vault; PB — pupillary block; TPI — tjhick peripheral block; ACD — anterior chamber depth; CAD — corneal arcuate distance; PD — pupil diameter; LV — lens vault; ACA — anterior chamber area; A.C. — anterior chamber volume; AOD — angle opening distance; ARA — angle recess area; TISA — trabecular irisspace area; TIA — trabecular iris angle; SSAngle — scleral spur angle; IT — iris thickness; IC — iris curvature; ICA— iris curvature area; IA — iris area

were the greatest in TPI (0.40 mm, 0.46 mm) and the lowest in LLV (0.31 mm) and PIC group (0.35 mm), respectively. IC and ICA were the highest in LLV (0.37 mm, 1.02 mm^2) and the lowest in the TPI group (0.26 mm, 0.61 mm^2).

The iris area (IA) showed no significant differences between groups.

To the best of our knowledge, this is the first report trying to differentiate the four PAC mechanisms using IC, ICA, and IA parameters in Caucasian eyes.

DISCUSSION

In this study, using ASOCT, we qualitatively recognized and quantitatively evaluated the four PAC mechanisms: PB, PIC, TPI, and LLV in Caucasian eyes. We tried to ascribe the obtained AC and AC angle parameters to these mechanisms. All four PAC mechanisms were defined in accordance with the literature. As mentioned before, this was strictly an ASOCT-based study. Thus, plateau iris configuration (PIC) refers only to the characteristic shape of the anterior surface of the iris observed on the ASOCT images.

Recent studies have described angle closure mechanisms based on ASOCT imaging. To date, no studies have evaluated different PAC mechanisms in the Caucasian population. Shabana et al. [13] have evaluated different PAC mechanisms and quantified the AC and AC angle parameters using ASOCT in the Asian population.

In the present study, 4 mechanisms of angle closure were identified. Our results showed that pupillary block (PB) was the dominant PAC mechanism in Caucasian eyes (57.6%), followed by PIC (29.2%) and TPI (9.7%). Pupillary block (PB) was the most frequent mechanism in our group. PB group was characterized by greater iris curvature, a small zone of iris lens contact in the center, and a shallow peripheral anterior chamber. Iris curvature has been proposed as an indicator of pupillary block. LLV was very rare in our group (3.5%). In the Asian population (Shabana et al.) LV was the most common PAC mechanism (35.8%), followed by PB (34.5%), PIC (15.5%) and TPI (14.2%).

In our study, eyes with PIC had the largest axial length and lowest spherical equivalent among all the 4 groups. Eyes in the LLV group had the shortest axial length. Our results are consistent with those of the Asian population (Shabana et al.). In our study, the spherical equivalent was the highest in the TPI and LLV groups. However, in the Asian population, the highest spherical equivalent was in the LLV and PB groups (Shabana et al.).

We found that both anterior chamber and anterior chamber angle parameters significantly differed in the four PAC mechanisms. In this study, anterior chamber parameters (ACD, ACA, and ACV) were highest in the PIC group and lowest in the LLV group, and the differences between these groups were statistically significant. Our results are consistent with those obtained in the Asian population (Shabana et al.).

The lens plays an important role in the pathogenesis of angle closure. It was shown that increased LV is strongly associated with angle closure, independently from the lens thickness and more anterior position of the lens. Moghimi et al. [14] evaluated ASOCT images of the eyes with PAC and demonstrated that exaggerated LV was responsible for a large proportion of acute primary angle closure (APAC). In our study, the LLV group was characterized by large LV and shallow AC. In our Caucasian group, LV was the highest in the large lens vault group and the lowest in the RI and IP group. This finding agrees with other studies (Shabana et al.), which also found the highest in the LLV group and the lowest in the PIC group. In our study PD was the highest in the TPI group and the lowest in the LLV and PIC groups. In the Asian population, LV was the highest in the TPI group and the lowest in the PIC group.

Our study showed that eyes with TPI had the thickest iris at both distances (IT750 and IT2000). Shabana et al. also showed the highest iris thickness in the TPI Asian group. Wang et al. [15] found that thicker iris, larger iris volume, and greater iris curvature are independently associated with narrow-angle. Nongpiur et al. [16] found that PACG eyes have a more prominent iris than PACS eyes. It was demonstrated that iris curvature decreases after LPI, but iris area does not. It was speculated that a larger iris area may be a risk factor for progressive angle closure once the pupillary block is eliminated after LPI. Our results show that IC and ICA were the highest in the LLV group and the lowest in the TPI group. A likely explanation for this is the anteriorly placed lens in the LLV group, though this group was small, and the measurements were susceptible to possible errors.

In this study, the plateau iris configuration group had higher anterior chamber parameters

(ACD, ACA, ACV) and anterior chamber angle parameters (AOD, ARA, TIA, TISA) at 500 and 750 μm than the pupillary block group. Eyes in the large lens vault group had lower anterior chamber parameters (ACD, ACA, ACV) than the pupillary block group. However, anterior chamber angle parameters (AOD, ARA, TIA, TISA) were higher in the large lens vault group than in the pupillary block group in our study.

The study of the Asian population (Shabana et al.) also showed the highest ACD parameters in the PIC group and the lowest ACD in the LLV group.

Although all angle parameters differed amongst four angle closure mechanisms, AOD 500, AOD 750, TIA 750, SSAngle 500, SSAngle 750 showed the strongest relevance ($p < 0.001$). Shabana et al. have suggested that measurements at a distance of 750 μm are more accurate than 500 μm due to the larger scan region being measured and lower susceptibility to iris irregularity. The results of our study support this hypothesis. Therefore, all angle parameters showed more significant differences in four PAC mechanisms at the distance 750 μm than 500 μm. It was found that AOD750 was the highest in the PIC group (0.23 mm) and the lowest in the TPI group (0.15 mm). In the Asian population, AOD750 parameter was also the highest in the PIC group (0.19 mm) and similar in the remaining groups (0.10, 0.11). TISA750, TIA750, and SSangle750 showed matching associations, with the highest being in the PIC group and the lowest in the TPI group, both in the Caucasian and Asian populations.

The characteristic contour of the iris in the PIC group is well described by the AOD parameter. This unique feature causes the most significant difference (0.06 mm) between AOD 750 and AOD 500, (0.05 mm) between TISA500 and TISA750, and 0.06mm between ARA500 and ARA 750 in all four groups. Considering that diagnostic criteria for *plateau iris* have not been well defined, this finding may play an important role in identifying *plateu iris* configuration and stands in agreement with other studies.

The lowest quantitative measurements were expected to describe the crowded angle in the TPI group. This shows that in this group, there is a probability of increased area of iridotrabecular contact during pupil dilation.

Many studies have reported that some eyes have residual angle closure despite the presence of a patent iridotomy [17–19]. In the eyes, other pathogenic mechanisms, such as plateau iris configuration, peripheral iris crowding, and forward movement of the lens, have also been suggested to contribute to the angle closure. Radhakrishnan [20] suggested that some ASOCT parameters, such as greater lens vault and thicker iris, are associated with persistent angle closure after LPI. These factors represent narrower angles before LPI and nonpupillary block mechanisms of angle closure.

The qualitative and quantitative information obtained from ASOCT imaging enables a better understanding of the underlying mechanisms of angle closure and provides functional parameters to tailor the treatment.

We are aware of certain limitations of our study. First, our results should be compared to those from the population-based study to develop more accurate qualitative parameters. Comparing a bigger number of eyes should allow us to highlight more differences among the four groups. UBM examination would provide more data about the ciliary body; however, we often rely on OCT scans only in everyday practice. Therefore, our study was designed to be the OCT study.

REFERENCES

1. Quigley HA, Broman AT. The number of people with glaucoma worldwide in 2010 and 2020. Br J Ophthalmol. 2006; 90(3): 262–267, doi: 10.1136/bjo.2005.081224, indexed in Pubmed: 16488940.
2. Day AC, Baio G. The prevalence of primary angle closure glaucoma in European derived popu- lations: A systematic review. Br J Ophthalmol. 2012; 96(9): 1162–1167, doi: 10.1136/bjophthalmol-2011-301189, indexed in Pubmed: 22653314.
3. Barkana Y, Dorairaj S, Tham YC, et al. Global prevalence of glaucoma and projections of glaucoma burden through 2040: a systematic review and meta-analysis. Ophthalmology. 2014; 121(11): 2081–2090, doi: 10.1016/j.ophtha.2014.05.013, indexed in Pubmed: 24974815.
4. Alsbirk PH. Anatomical risk factors in primary angle-closure glaucoma. A ten year follow up survey based on limbal and axial anterior chamber depths in a high risk population. Int Ophthalmol. 1992; 16(4-5): 265–272, doi: 10.1007/BF00917973, indexed in Pubmed: 1428555.
5. Li H, Leung CK, Cheung CY, et al. Repeatability and reproducibility of anterior chamber angle measurement with anterior segment optical coherence tomography. Br J Ophthalmol. 2007; 91(11): 1490–1492, doi: 10.1136/bjo.2007.118901, indexed in Pubmed: 17475709.
6. Müller M, Dahmen G, Pörksen E, et al. Anterior chamber angle measurement with optical coherence tomography: intraobserver and interobserver variability. J Cataract Refract Surg. 2006; 32(11): 1803–1808, doi: 10.1016/j.jcrs.2006.07.014, indexed in Pubmed: 17081861.
7. Radhakrishnan S, See J, Smith S, et al. Reproducibility of Anterior Chamber Angle Measurements Obtained with Anterior Segment Optical Coherence Tomography. Invest Ophthalmol Vis Sci . 2007; 48(8): 3683–3688, doi: 10.1167/iovs.06-1120, indexed in Pubmed: 17652739.

8. Aung T, Nolan WP, Machin D, et al. Anterior chamber depth and the risk of primary angle closure in 2 East Asian populations. Arch Ophthalmol. 2005; 123(4): 527–532, doi: 10.1001/archopht.123.4.527, indexed in Pubmed: 15824227.
9. Gupta B, Angmo D, Yadav S, et al. Ocular parameters in the subgroups of angle closure glaucoma. Clin Exp Ophthalmol. 2000; 28(4): 253–258, doi: 10.1046/j.1442-9071.2000.00324.x, indexed in Pubmed: 11021552.
10. Amerasinghe N, Aung T. Angle-closure: risk factors, diagnosis and treatment. Prog Brain Res. 2008; 173: 31–45, doi: 10.1016/S0079-6123(08)01104-7, indexed in Pubmed: 18929100.
11. Guzman CP, Gong T, Nongpiur ME, et al. Anterior segment optical coherence tomography parameters in subtypes of primary angle closure. Invest Ophthalmol Vis Sci. 2013; 54(8): 5281–5286, doi: 10.1167/iovs.13-12285, indexed in Pubmed: 23788370.
12. Shabana N, Aquino MCD, See J, et al. Quantitative evaluation of anterior chamber parameters using anterior segment optical coherence tomography in primary angle closure mechanisms. Clin Exp Ophthalmol. 2012; 40(8): 792–801, doi: 10.1111/j.1442-9071.2012.02805.x, indexed in Pubmed: 22594402.
13. Moghimi S, Chen R, Hamzeh N, et al. Qualitative evaluation of anterior segment in angle closure disease using anterior segment optical coherence tomography. J Curr Ophthalmol. 2016; 28(4): 170–175, doi: 10.1016/j.joco.2016.06.005, indexed in Pubmed: 27830199.
14. Wang BS, Narayanaswamy A, Amerasinghe N, et al. Increased iris thickness and association with primary angle closure glaucoma. Br J Ophthalmol. 2011; 95(1): 46–50, doi: 10.1136/bjo.2009.178129, indexed in Pubmed: 20530187.
15. Nongpiur M, Atalay E. Anterior segment imaging-based subdivision of subjects with primary angle-closure glaucoma. Eye. 2017; 31: 572–577, doi: 10.1038/eye.2016.267, indexed in Pubmed: 27935603.
16. Baskaran M, Yang E, Trikha S, et al. Residual Angle Closure One Year After Laser Peripheral Iridotomy in Primary Angle Closure Suspects. Am J Ophthalmol. 2017; 183: 111–117, doi: 10.1016/j.ajo.2017.08.016, indexed in Pubmed: 28887116.
17. He M, Friedman DS, et al. Laser peripheral iridotomy in primary angle-closure suspects: bio- metric and gonioscopic outcomes: the Liwan Eye Study. Ophthalmology. 2007; 114(3): 494–500, doi: 10.1016/j.ophtha.2006.06.053, indexed in Pubmed: 17123610.
18. Lee KS, Sung KR, Kang SY, et al. Residual anterior chamber angle closure in narrow-angle eyes following laser peripheral iridotomy: anterior segment optical coherence tomography quantitative study. Jpn J Ophthalmol. 2011; 55(3): 213–219, doi: 10.1007/s10384-011-0009-3, indexed in Pubmed: 21559907.
19. Leffler CT, Radhakrishnan S, Chen PP, et al. Laser Peripheral Iridotomy in Primary Angle Closure: A Report by the American Academy of Ophthalmology. Ophthalmology. 2018; 125(7): 1110–1120, doi: 10.1016/j.ophtha.2018.01.015, indexed in Pubmed: 29482864.
20. Wright C, Tawfik MA, Waisbourd M, et al. Primary angle-closure glaucoma: an update. Acta Ophthalmol. 2016; 94(3): 217–225, doi: 10.1111/aos.12784, indexed in Pubmed: 26119516.